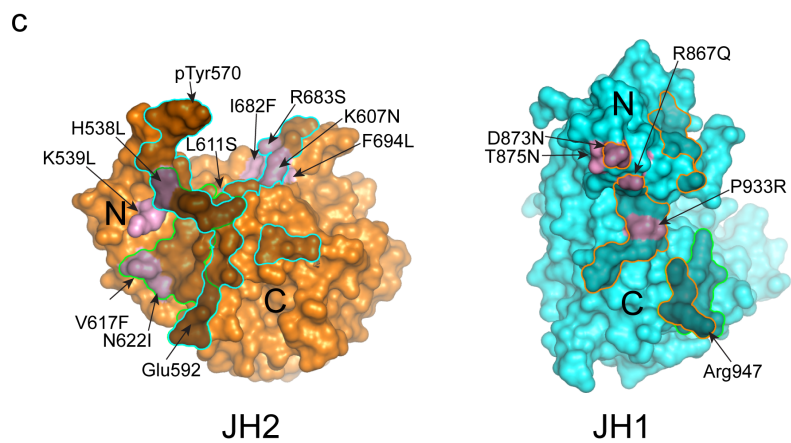
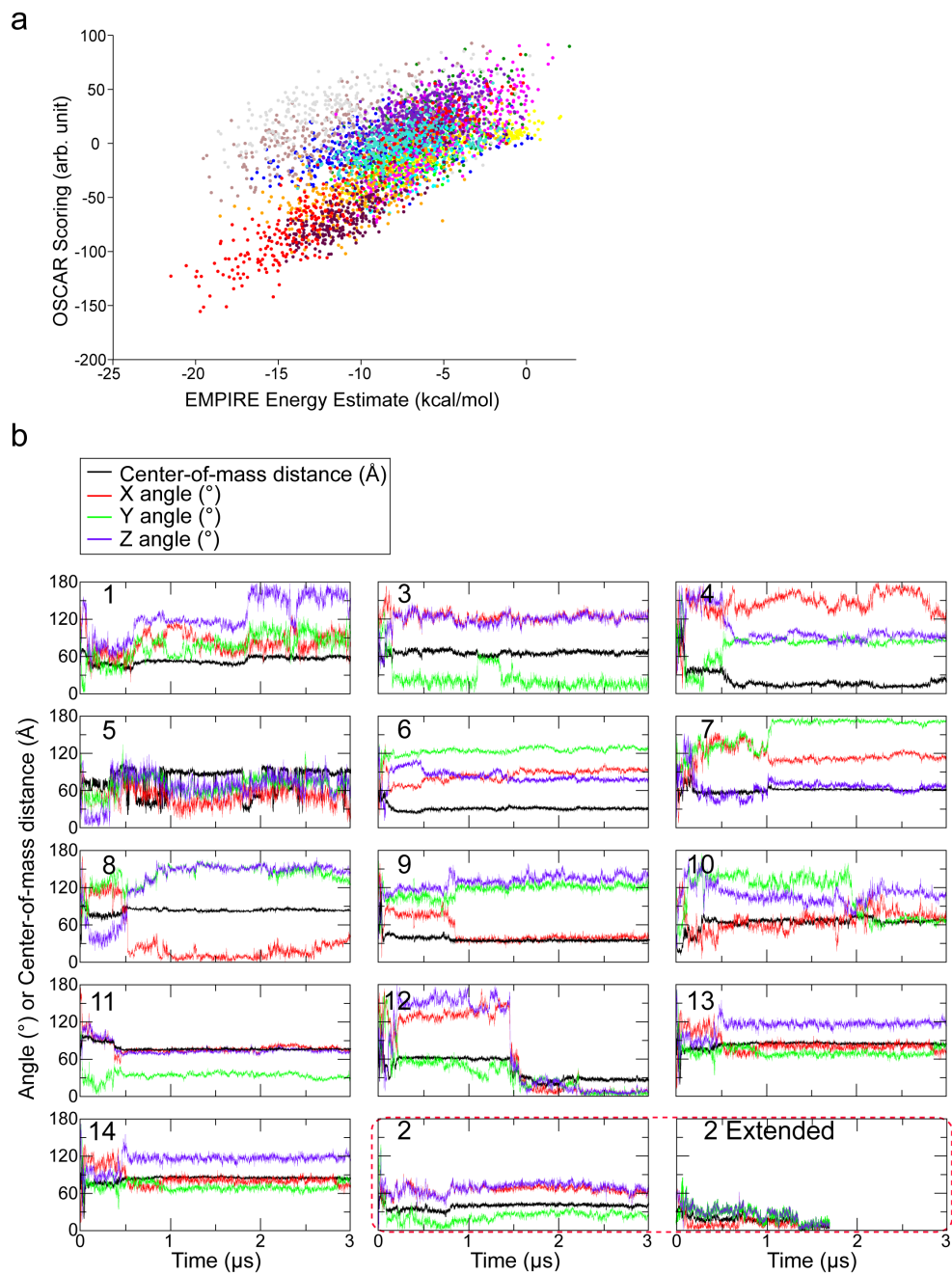


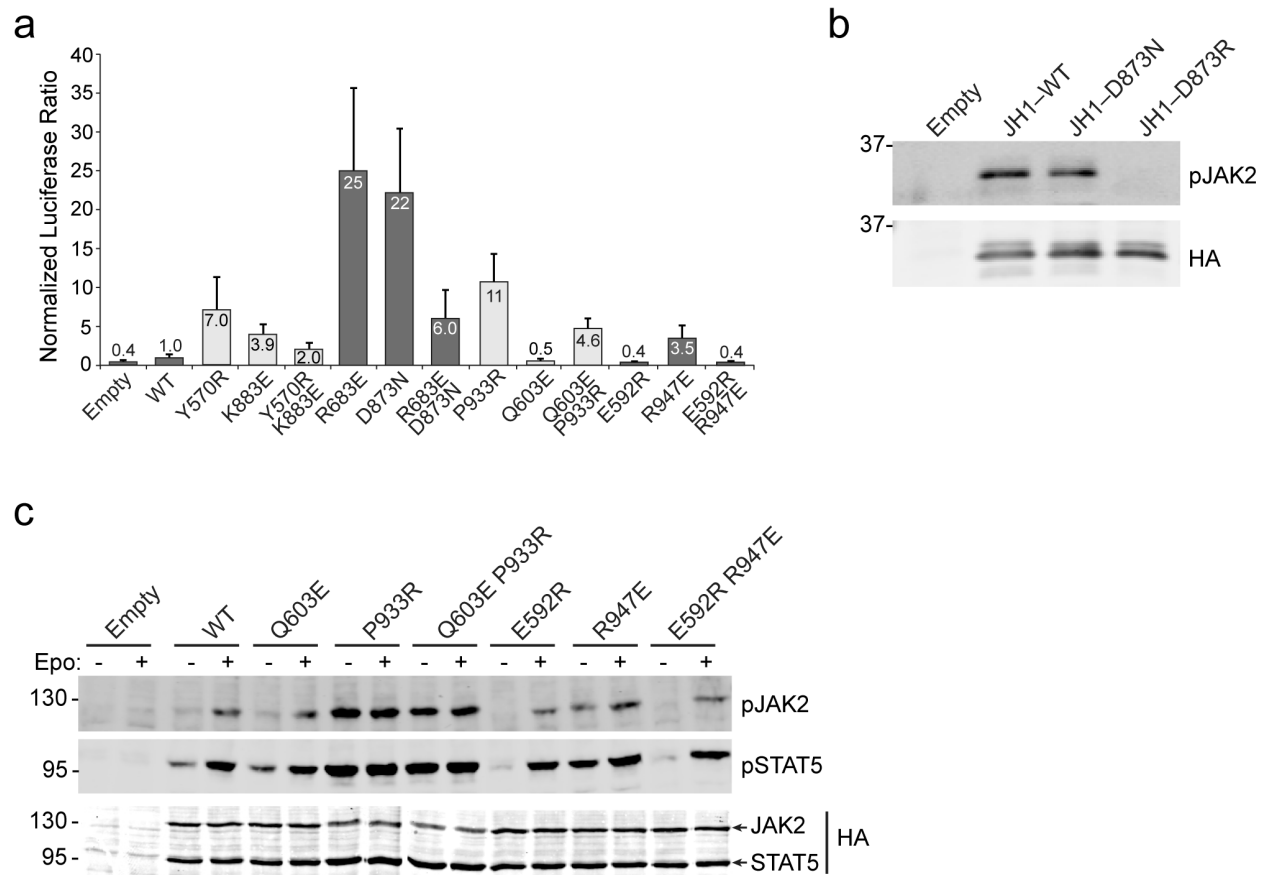
## **Molecular basis for pseudokinase-dependent autoinhibition of JAK2 tyrosine kinase**

Yibing Shan, Kavitha Gnanasambandan, Daniela Ungureanu, Eric T. Kim, Henrik Hammarén,  
Kazuo Yamashita, Olli Silvennoinen, David E. Shaw, and  
Stevan R. Hubbard

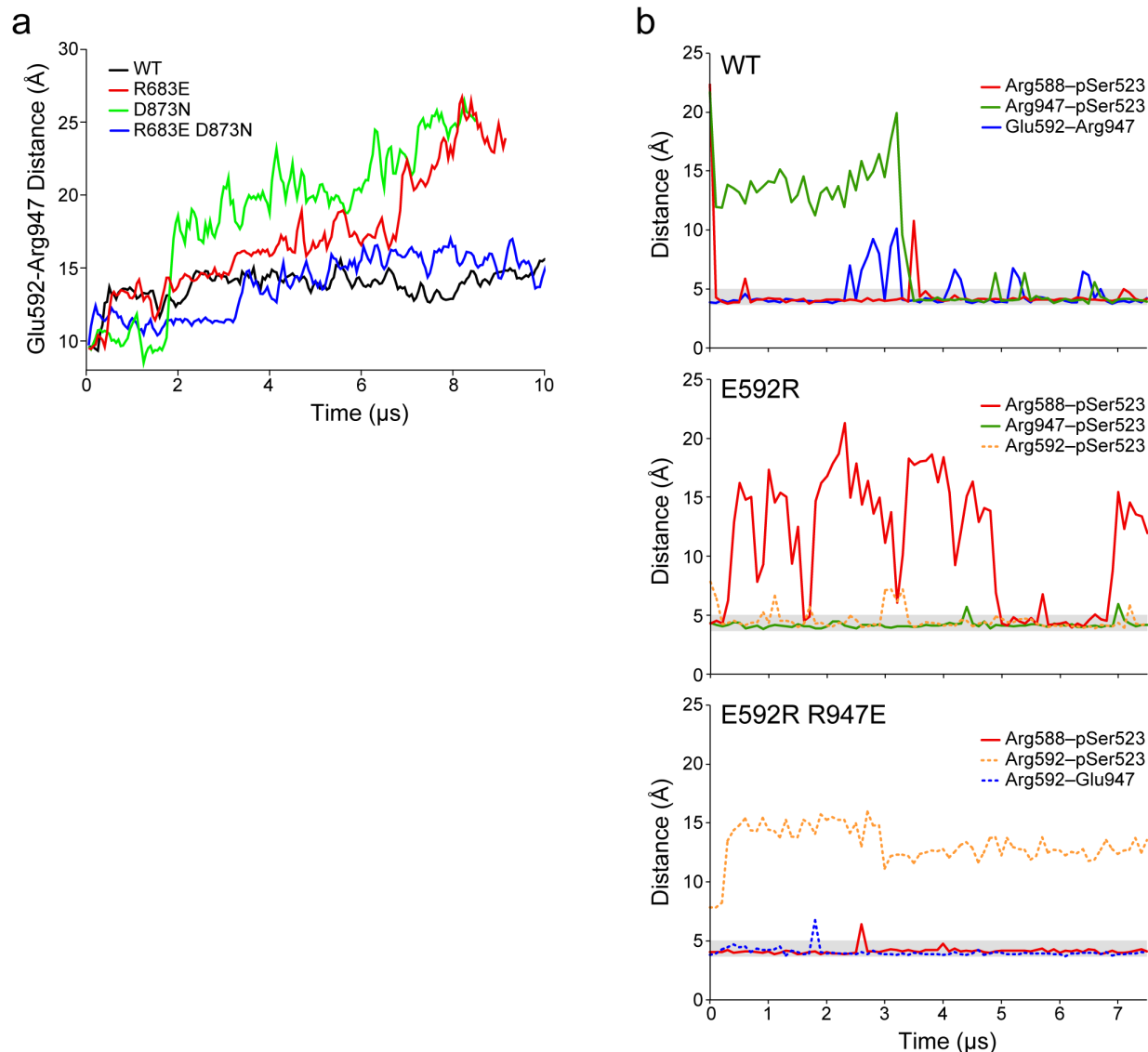
This PDF includes Supplementary Figures 1–6.



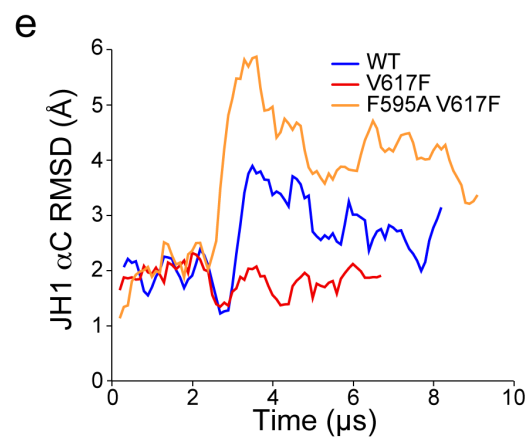
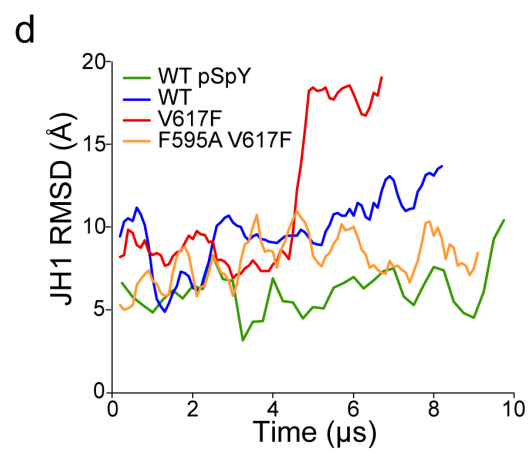
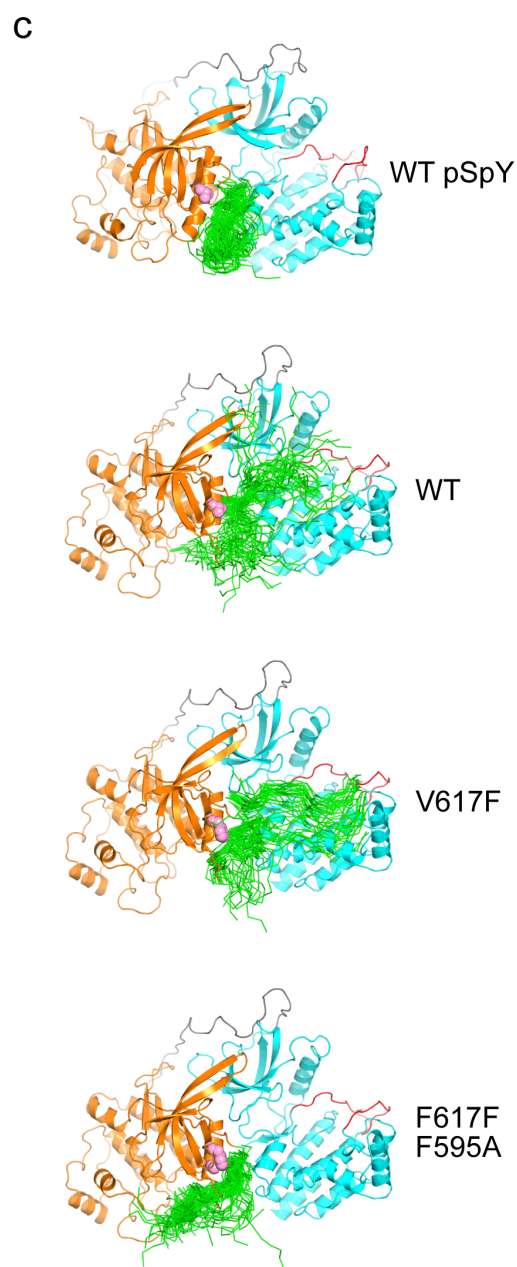
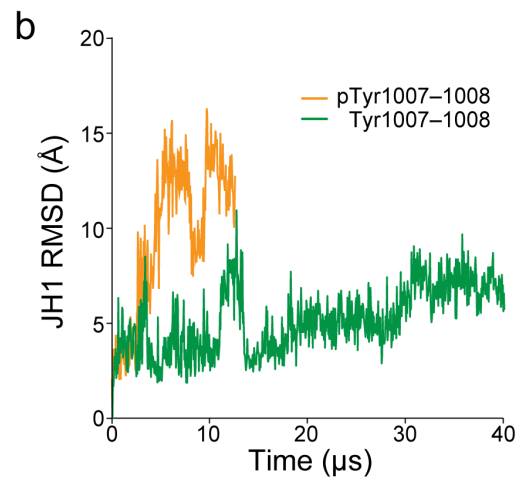
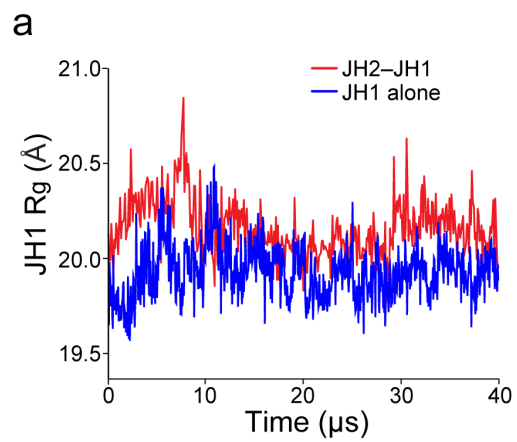
**Supplementary Figure 1** (a) Analysis of 14 JAK2 JH2–JH1 poses. From each of the 14 3.0- $\mu$ s simulations, starting from an arbitrary JH2–JH1 non-contacting pose, 300 snapshots (10-ns interval) were evaluated using both EMPIRE and OSCAR scoring functions<sup>3,4</sup>. The score of each snapshot from each simulation was plotted in the two-dimensional energy space with a unique color. The dots corresponding to the simulation that generated pose 2, the JH2–JH1 interaction that was pursued further (see Fig. 1), are colored red. (b) Time evolution of the orientation of JH1 and its center of mass for each of the 14 initial simulations (see Fig. 1). For each time snapshot in the simulations, the JH1 orientation is represented by the angles of the JH1 principal axes of inertia relative to the principal axes of JH1 in the final model. Also shown for each snapshot is the distance of the JH1 center-of-mass from the JH1 center-of-mass in the final model. JH2 in each snapshot is superimposed on JH2 in the final model prior to the angle and distance calculations. As shown, pose 2 (end of simulation 2) bears resemblance to, but is non-trivially different from the pose in the final model. Only after addition of the JH2–JH1 linker and further simulation (‘2 Extended’) does this pose converge towards the final model. Other than simulation 2, simulation 12 also reached a JH2–JH1 pose that bears resemblance to the pose in the final model. (c) Surface representations of JH2 (left) and JH1 (right) in “open book” view, in which JH2 has been rotated clockwise by 90° (vertical axis) and JH1 counterclockwise by 90°, with respect to the orientation in Fig. 1a, to reveal the interaction surface. Left: in cyan outline are residues in JH2 (residues 537 to 810) that are within 4.0 Å of an atom in JH1, and in green outline are residues in JH2 that are within 4.0 Å of an atom in the SH2–JH2 linker (residues 520–536). Right: same as left, except for JH1 (residues 840–1132) relative to JH2 (orange outline) and the SH2–JH2 linker (green outline). Activating mutations in JH1 and JH2 are colored pink and labeled. Other residues of interest are also labeled, as are the N and C lobes of the kinase domains.



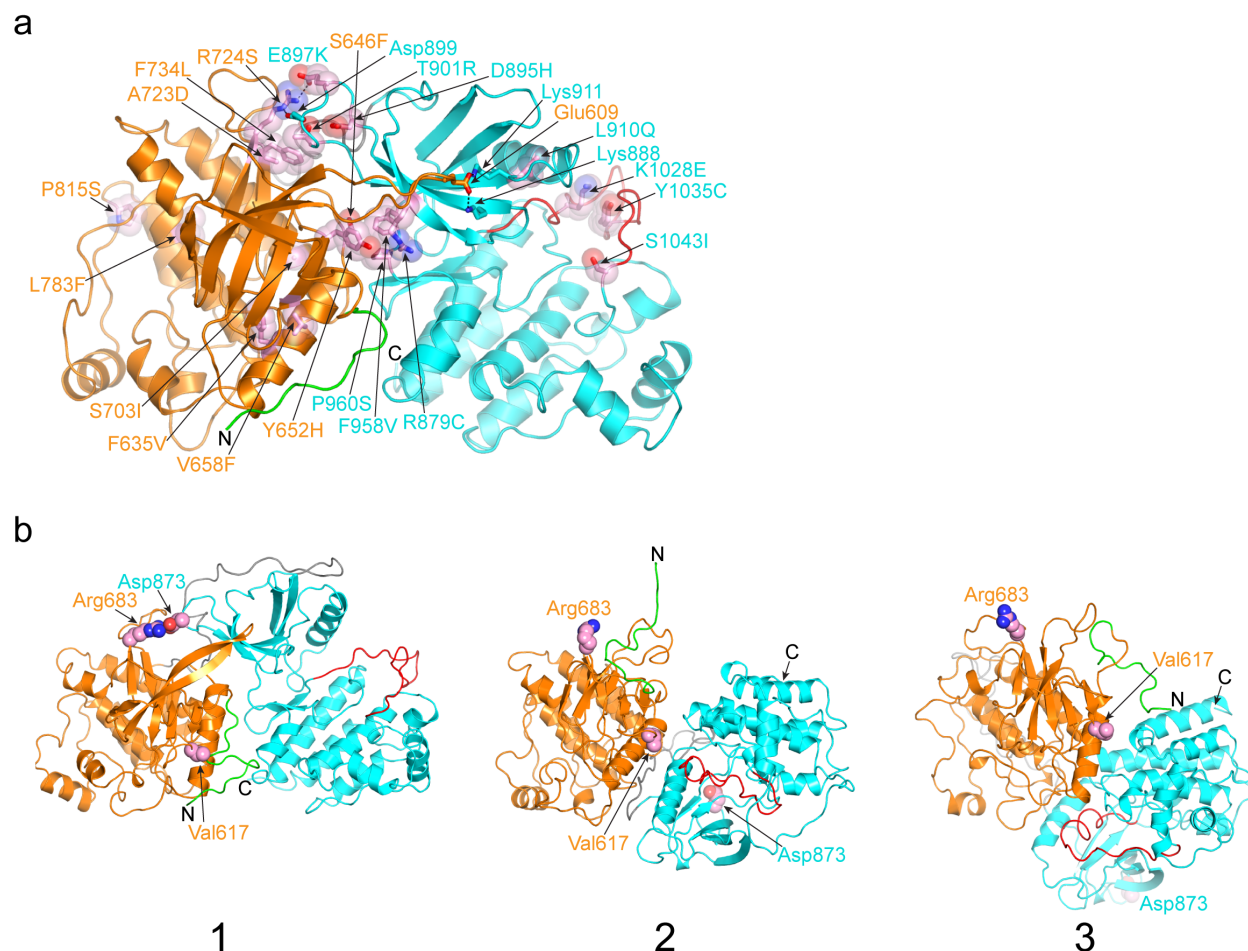
**Supplementary Figure 2** Functional studies of JAK2 mutants. **(a)** Luciferase activities of wild-type and mutant JAK2 measured using an APRE-luc reporter to assess endogenous STAT3-dependent transcription in COS7 cells. The firefly luciferase activity of each sample was normalized to that of renilla luciferase (luciferase ratio) and plotted as fold-change relative to the wild-type JAK2 (WT) luciferase ratio (set to 1.0). Average values and standard deviations were derived from triplicate samples (N=3). **(b)** Analysis of JAK2 mutants D873R and D873N in JH1 alone. Representative western blot of JAK2 JH1 (HA-tagged) immunoprecipitated from transfected HEK 293T cells and probed for JAK2 Tyr1007–1008 phosphorylation (pJAK2) (top) or protein levels (HA) (bottom). A reference molecular-weight marker (in kDa) is indicated on the left. **(c)** Epo-dependent activation of JAK2 mutants. JAK2-deficient  $\gamma$ 2A cells transfected with the indicated JAK2 and STAT5 (HA-tagged) plasmids were either left untreated (–) or stimulated with Epo (+), and the whole cell lysates were probed for JAK2 Tyr1007–1008 phosphorylation (pJAK2, top), STAT5 phosphorylation (pSTAT5, middle), or protein levels (HA, bottom). Reference molecular-weight markers (in kDa) are indicated on the left.



**Supplementary Figure 3** Simulations of JAK2 JH2-JH1 mutants. **(a)** Analysis of R683E, D873N and R683E D873N. The distance between the C $\alpha$  atoms of Glu592 (JH2) and Arg947 (JH1), interacting residues in the JH2-JH1 model (see Fig. 2e), is plotted as a function of simulation time. In the activating mutations R683E and D873N, the two residues (Glu592, Arg947) separated, whereas for wild type (WT) and the double mutation, the distance remained relatively stable. **(b)** Salt-bridge analysis for JAK2 Glu592-Arg947. WT, E592R, and E592R R947E, were simulated for 7.5  $\mu$ s each. Plotted are the distances between select residues as a function of simulation time. Shown in solid lines are the distance trajectories between native residues, and shown in dashed lines are distance trajectories in which at least one of the residues involved has been introduced by mutation. To simplify the salt-bridge presentation, the actual distances displayed are between C $\zeta$  of Arg588, Arg592, or Arg947 (to account for N $\epsilon$ , N $\eta$ 1, and N $\eta$ 2 of arginine) and either C $\delta$  of Glu592 or Glu947 (to account for O $\epsilon$ 1 and O $\epsilon$ 2 of glutamic acid) or P of pSer523 (to account for O1P, O2P, and O3P of phosphoserine). Thus, the representative distance for a salt bridge is  $\sim$ 3.8 Å rather than  $\sim$ 2.7 Å (typical nitrogen-oxygen distance). Gray rectangles indicate the approximate distance range for salt bridges.



**Supplementary Figure 4** Conformational changes in JH1 and analysis of V617F. **(a)** Radius of gyration ( $R_g$ , an overall measure of the size) of JH1 as a function of simulation time (same simulations as in Fig. 4a). **(b)** RMSD for  $C\alpha$  atoms in JH1 as a function of simulation time, after aligning  $C\alpha$  atoms in JH2 for each time frame with the  $C\alpha$  atoms in their initial positions. Both simulations were initiated from an identical JH2–JH1 pose with Ser523 and Tyr570 phosphorylated. In one simulation (orange), the JH1 activation loop was phosphorylated at Tyr1007 and Tyr1008, and in the other simulation (green), the activation loop was unphosphorylated. A high RMSD is indicative of a high degree of structural deviation from the JH2–JH1 configuration (the autoinhibitory pose) shown in Fig. 2a. **(c–e)** Analyses of JAK2 MPN mutation V617F. In previous studies, we showed that Ser523 and Tyr570 are poorly phosphorylated in activated JAK2 mutants such as V617F<sup>5</sup>. Thus, to simulate V617F JH2–JH1 properly, we left Ser523 (and Tyr570) unphosphorylated and, for comparison purposes, we also simulated unphosphorylated wild type ('WT'). F595A, in  $\alpha C$  of JH2 and proximal to Val617, was shown to suppress V617F<sup>8,9</sup>, and therefore we also simulated F595A V617F (unphosphorylated). **(c)** The SH2–JH2 linker conformations visited during the simulations. JH2–JH1 in the first time frame ( $t=0$ ) of each trajectory is shown in ribbon representation and colored as in Fig. 1. The  $C\alpha$  trace of the SH2–JH2 linker (residues 522–536) for each time frame is shown in green, after aligning JH2 in each frame with JH2 at  $t=0$ . As shown, the linker in V617F is least stable in the binding groove between JH2 and JH1. **(d)** RMSD for  $C\alpha$  atoms in JH1 as a function of simulation time, after aligning  $C\alpha$  atoms in JH2 for each time frame with the  $C\alpha$  atoms in their initial positions. Removal of pSer523 and pTyr570 ('WT' versus 'WT pSpY') led to an increase in the overall conformational heterogeneity of JH1 and thus destabilization of the JH2–JH1 complex. V617F caused a further increase in JH1 heterogeneity, and addition of F595A to V617F restored JH1 heterogeneity back to the level of phosphorylated JH2–JH1 ('WT pSpY'). **(e)** RMSD for  $C\alpha$  atoms in  $\alpha C$  of JH1 (residues 889–904) relative to the active conformation, after aligning all the  $C\alpha$  atoms in JH1. As shown, the active conformation of  $\alpha C$  is most stable in V617F.



**Supplementary Figure 5** JAK1 JH2–JH1 model and comparison of JAK JH2–JH1 models. **(a)** Atomic models of JAK1 JH2 (PDB code 4L00 (ref. 1)) and JH1 (PDB code 4E5W (ref. 2)) were placed by superposition into the positions of JH2 and JH1 of JAK2 (Fig. 2a). The SH2–JH2 and JH2–JH1 linkers were added, and an MD simulation was run for 12  $\mu$ s. Shown is a representative pose near the end of the simulation. JH2 (residues 575–850) is colored orange, JH1 (residues 866–1154) is colored cyan, with the activation loop (residues 1021–1043) colored red, the SH2–JH2 linker (residues 563–574) is colored green, and the JH2–JH1 linker (residues 851–865) is colored gray. Mapped activating mutations<sup>43</sup> are shown in stick representation, colored pink, and labeled. Other residues of interest are shown in stick representation and labeled. The N-terminus (residue 563) is labeled ‘N’, and the C-terminus (residue 1154) is labeled ‘C’. **(b)** Ribbon diagram of the JAK2 JH2–JH1 model from the current study (1), from Lindauer et al.<sup>6</sup> (2), and from Wan et al.<sup>7</sup> (3). Coloring is the same as in Fig. 1. The side chains of Val617, Arg683, and Asp873 are shown in sphere representation and colored pink (carbon atoms). The models are aligned with one another based on a superposition of JH2. The N- and C-termini for each model are labeled ‘N’ and ‘C’.

Fig. 3a pJAK2

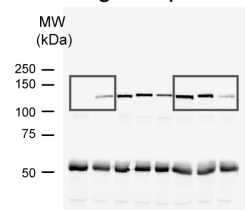


Fig. 3a HA

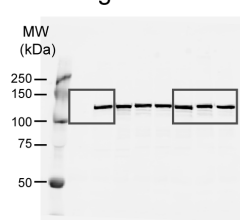


Fig. 3a,d pSTAT1

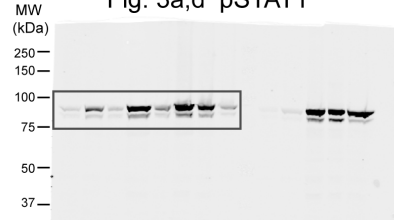


Fig. 3b pJAK2

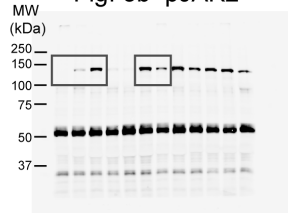


Fig. 3b HA

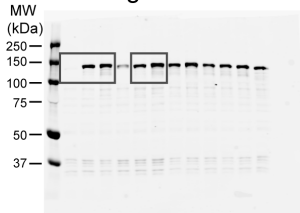


Fig. 3b pSTAT1

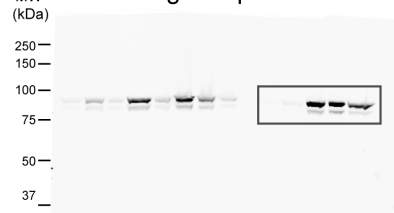


Fig. 3c pJAK2

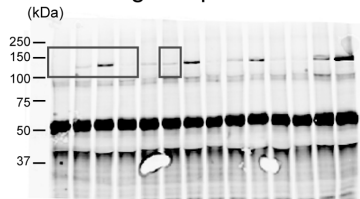


Fig. 3c HA

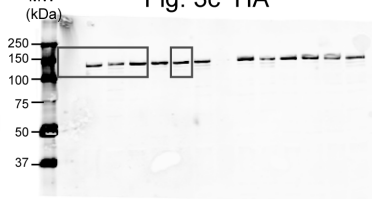


Fig. 3a,b,d STAT1

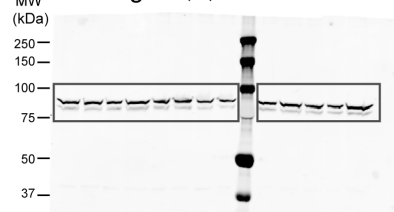


Fig. 3d pJAK2

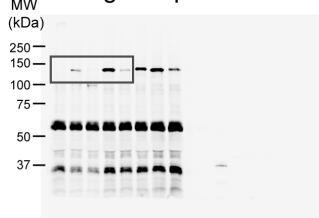


Fig. 3d HA

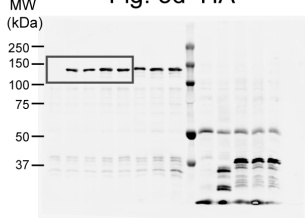


Fig. 3c pSTAT1

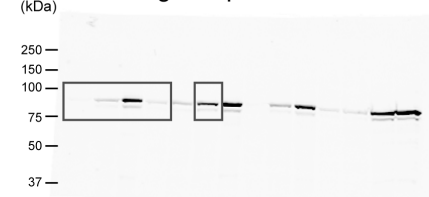
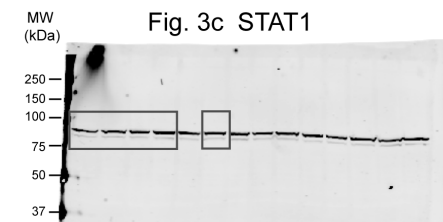


Fig. 3c STAT1



**Supplementary Figure 6** Uncropped images for western blots shown in Fig. 3. For each blot (labeled accordingly), boxes mark the borders of the cropped images shown in Fig. 3.

## REFERENCES

1. Liang, S., Liu, S., Zhang, C. & Zhou, Y. A simple reference state makes a significant improvement in near-native selections from structurally refined docking decoys. *Proteins* **69**, 244-253 (2007).
2. Liang, S., Zhang, C., Sarmiento, J. & Standley, D.M. Protein loop modeling with optimized backbone potential functions. *J. Chem. Theor. Comp.* **8**, 1820-1827 (2012).
3. Ungureanu, D., *et al.* The pseudokinase domain of JAK2 is a dual-specificity protein kinase that negatively regulates cytokine signaling. *Nat. Struct. Mol. Biol.* **18**, 971-976 (2011).
4. Dusa, A., Mouton, C., Pecquet, C., Herman, M. & Constantinescu, S.N. JAK2 V617F constitutive activation requires JH2 residue F595: a pseudokinase domain target for specific inhibitors. *PLoS One* **5**, e11157 (2010).
5. Gnanasambandan, K., Magis, A. & Sayeski, P.P. The constitutive activation of Jak2-V617F is mediated by a pi stacking mechanism involving phenylalanines 595 and 617. *Biochemistry* **49**, 9972-9984 (2010).
6. Toms, A.V., *et al.* Structure of a pseudokinase-domain switch that controls oncogenic activation of Jak kinases. *Nat. Struct. Mol. Biol.* **20**, 1221-1223 (2013).
7. Kulagowski, J.J., *et al.* Identification of imidazo-pyrrolopyridines as novel and potent JAK1 inhibitors. *J. Med. Chem.* **55**, 5901-5921 (2012).
8. Lindauer, K., Loerting, T., Liedl, K.R. & Kroemer, R.T. Prediction of the structure of human Janus kinase 2 (JAK2) comprising the two carboxy-terminal domains reveals a mechanism for autoregulation. *Protein Eng.* **14**, 27-37 (2001).
9. Wan, X., Ma, Y., McClendon, C.L., Huang, L.J. & Huang, N. Ab Initio Modeling and Experimental Assessment of Janus Kinase 2 (JAK2) Kinase-Pseudokinase Complex Structure. *PLoS Comput. Biol.* **9**, e1003022 (2013).